Mathematical and computational modelling of the dynamic behaviour of direct current plasma arcs

by Q.G. Reynolds*, R.T. Jones*, and B.D. Reddy†

Synopsis

The problem of direct-current plasma arc behaviour, interaction, and dynamics is considered in the context of metallurgical DC arc furnace applications. Particular attention is paid to the transient flow behaviour of arc systems. A mathematical formulation of the physics used to describe the arc system is presented, and includes the spatial and temporal evolution of fluid flow, heat transfer, and electromagnetism. Based on this formulation, a numerical model is developed using a finite difference approach on a regular cartesian grid in both two and three dimensions, with a special focus on robust stability, high resolution modelling, and high performance.

A collection of results produced using the numerical model to study pilot plant-scale furnaces is then presented. These address a range of process and design variables and their effect on the numerical model's results. Where possible, the qualitative behaviour of the model is compared to available experimental data. A number of novel effects and phenomena are seen in the dynamic behaviour of the DC plasma arc model for both single and multiple arc systems, which may lead to improved understanding, control, and manipulation of such systems where they occur in industrial applications.

Keywords
Pyrometallurgy, direct-current furnace, plasma arc, modelling.

Introduction

Research and development into the use of the direct current arc furnace (DCAF) as an environmentally cleaner and more energy-efficient alternative for pyrometallurgical processes is an area of active study. To date, large scale pilot-plant work has been successfully performed on ferrochrome, ferronickel, magnesium, titanium dioxide, platinum group metals, zinc, and many others[1–5]. Industrial-scale commercialization of several of these processes has been realized.

The DCAF (see Figure 1) typically consists of a cylindrical containment vessel, lined with cooling elements and refractory materials. A single electrode made of graphite enters the vessel from above. Raw feed material is fed into the vessel, usually via ports in the roof, and is heated to the point of melting by electrical power input to the furnace from a rectified direct current power supply. Chemical reductants, introduced concurrently with the feed, are then able to react very rapidly with the molten material to produce the desired product.

The principal energy source of the furnace is a direct-current plasma arc, which is struck between the end of the graphite electrode and the surface of the electrically conductive molten bath. The plasma arc functions by raising the temperature of the gas between the electrode and the molten bath via ohmic heating. Once the temperature of the gas is sufficiently high, its constituent molecules and atoms begin to ionize into positively charged ions and negatively charged electrons, giving a neutral but very strongly conductive plasma gas. This conducting material permits electrical current to pass from the furnace electrode through to the furnace bath and complete the circuit. Energy escapes from the arc via a multitude of mechanisms, most importantly thermal radiation from the hot plasma gas, and convection to the molten bath surface. Since much of this energy is delivered to a localized area directly beneath the arc, it is a very efficient way of heating the process material.

Flow of the plasma gas in the arc column is driven very strongly by electromagnetic forces, and tends to be directed downward in a jet from the electrode toward the molten bath due to the geometry of the arc attachment spot on the graphite electrode and the accelerating effect of the Lorentz force near the electrode (the Maecker effect[6]).

An understanding of the fundamental behaviour of DC plasma arcs is extremely valuable, as they are central to the operation of the DCAF. Of particular interest in this work is the nature of the dynamic behaviour of the arc, and its interaction with other arcs in the case of multiple-electrode furnaces.

* *Mintek, Randburg, South Africa.*

† *CERECAM, University of Cape Town, Rondebosch, South Africa.*

Transaction Paper

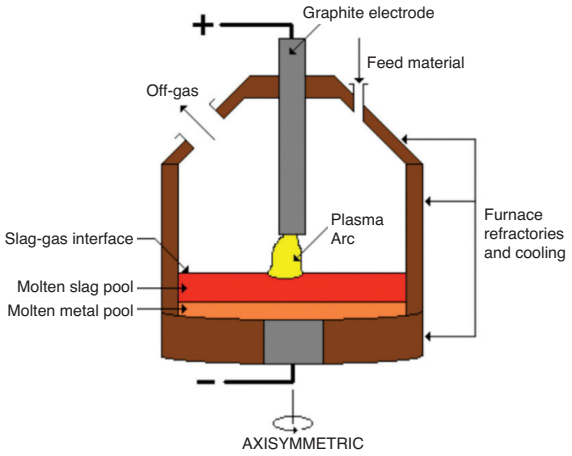

Figure 1—Schematic of DC arc furnace

Model development

Due to the tightly coupled multi-physics nature of the DC plasma arc problem, mathematical relationships governing the fluid dynamics, heat transfer, and electromagnetic fields occurring in arcs must be derived and solved simultaneously in order to accurately model the overall behaviour of the system.

Mathematical description

The arc is a high velocity gas jet driven by interactions with other physical phenomena, and is fundamentally a fluid flow problem. For simplicity and in order to focus on the dynamics of the system, incompressible flow with constant physical and transport properties is assumed. The Navier-Stokes equations then simplify to:

$$\frac{\partial \boldsymbol{v}}{\partial t} + (\boldsymbol{v}\cdot\nabla)\boldsymbol{v} + \nabla p = \frac{\mu}{\rho}\nabla^2\boldsymbol{v} + \frac{\boldsymbol{j}\times\boldsymbol{B}}{\rho} \quad [1]$$

$$\nabla\cdot\boldsymbol{v} = 0 \quad [2]$$

Here, v is the fluid velocity, ρ is the fluid density, p is the reduced pressure (P/ρ), μ is the kinematic viscosity, $\boldsymbol{j}$ is the electric current density vector, and B is the magnetic field.

The heat transfer model is similarly derived by assuming constant properties and making use of the local thermodynamic equilibrium approximation[7], by which a single temperature can be used to characterize the material's properties. The heat transfer model is given by the following expressions.

$$\frac{\partial T}{\partial t} + \boldsymbol{v}\cdot\nabla T = \frac{\kappa}{\rho C_p} \quad [3]$$

$$Q = \frac{\boldsymbol{j}\cdot\boldsymbol{j}}{\sigma} - Q_r \quad [4]$$

Here, T is the plasma temperature, C_p is the heat capacity at constant pressure, κ is the thermal conductivity, σ is the plasma electrical conductivity, and Q_r is the radiation energy loss per unit volume. It is important to note that the temperature dependence of both σ and Q_r is retained in the model. These values and their variation with temperature are essential to the formation of a sustained plasma arc.

Behaviour of the electrical and magnetic fields is governed by Maxwell's equations[8]. For the problem of plasma arcs, the timescales of interest are typically long in comparison to the propagation time of electromagnetic waves, and the simplified magnetostatic and electrostatic versions of the laws may be used.

$$\nabla\cdot(\sigma\nabla\phi) = 0 \quad [5]$$

$$\boldsymbol{j} = -\sigma\nabla\phi \quad [6]$$

$$\nabla^2\boldsymbol{A} = -\mu_0\boldsymbol{j} \quad [7]$$

$$\boldsymbol{B} = \nabla\times\boldsymbol{A} \quad [8]$$

Here, ϕ is the electrostatic potential, A is the auxiliary magnetic field, and μ_0 is the permeability of free space. As the arcs studied here are relatively small (2kA and lower), induced current transport terms in [6] have been ignored, leaving only the electrostatic current. Boundary conditions are provided for A by assuming that the boundaries of the region are magnetically insulating.

This set of equations fully describes the fundamental physics that govern the behaviour of the arc system, albeit in a greatly approximated fashion. The key element in this formulation is the retention of the time dependence of all transport equations, permitting the temporal evolution of the arc to be modelled.

Numerical method

The numerical treatment of the governing equations of the problem focuses on high spatial and temporal resolution, as well as high performance. Due to these and other factors many of the more contemporary approaches commonly used for the numerical solution of transport problems—such as finite volume or finite element techniques using unstructured grids—were rejected in favour of a simplified time-explicit finite difference method.

A novel formulation of the fluid flow equations due to E and Liu[9], the gauge method, is used in order to make [1] and [2] more amenable to numerical analysis. The gauge method introduces an additional auxiliary vector field related to the velocity and replaces pressure with a gauge variable, while remaining mathematically equivalent to the Navier-Stokes equations. This has the effect of alleviating many of the numerical complications associated with treatment of the pressure terms in primitive variable formulations such as MAC and projection methods.

The spatial discretization is performed on a two- or three-dimensional cartesian mesh, with grid points spaced equally in the direction of the x and y (and z if 3D) axes. A classical MAC staggered grid is used for the components of the velocity as well as the auxiliary vector field in the gauge scheme. Partial derivatives are then approximated with second order centred difference finite differences to yield numerical equations describing the relationships between neighbouring grid points.

It is important to note that a large proportion of the existing DC plasma arc modelling literature has made use of axisymmetric coordinate systems when working in two dimensions. Unfortunately, the enforced rotational symmetry means that while such systems may be more physically

realistic than a 2D cartesian grid for the problem of modelling the arc jet at steady state, they are unable to capture significant aspects of the arc dynamics that break its rotational symmetry, such as oscillations and twisted/helical column formation. They are also poorly suited to the study of multiple interacting arcs. In short, the axisymmetric coordinate system is valuable for time-averaged engineering models of single arcs, but less useful for more detailed dynamic studies.

The fluid flow and heat transfer equations are solved explicitly in the time variable. The traditional constraints on cell Reynolds number that arise from using centered difference approximations together with explicit time solvers are avoided by using a fourth order Runge-Kutta (RK4) calculation for the forward time step in both the fluid flow and heat transfer equations. As described by E and Liu[10] the use of high order explicit time step algorithms, including classical RK4, completely stabilizes the scheme if certain lenient constraints on the time step and grid dimensions are satisfied. The time step size is controlled adaptively throughout the calculation using these constraints.

At each step of the RK4 calculation, a single Poisson equation must be solved for the gauge variable in the fluid flow formulation. Additionally, at the end of every time step, [5] and [7] must be solved to obtain the electric potential and auxiliary magnetic field. For Poisson-like equations with simple boundary conditions, a rapid direct spectral solver based on the FFTW algorithm[11] is utilized. The electric potential equation has non-constant coefficients, and is instead solved using an iterative multigrid[12] solver.

Domain geometry and model parameters

A finite region immediately surrounding the arc in the central area of the furnace is modelled, consisting of the gas space between the bottom surface of the graphite electrode, and the top surface of the molten bath that forms the anode. The domain is rectangular in shape. This is depicted in Figure 2.

The origin of a cartesian coordinate system is placed at point *H*. The height of the domain is given by $y_{AH} = y_{FG}$, and the width is given by $x_{GH} = x_{AF}$. The molten bath anode is placed at the boundary *GH*. The surface of the graphite electrode is defined by the boundary *BE*, and the cathode spot which forms the root of the arc column is given by the boundary *CD*.

In order to completely specify a particular model case, several pieces of information must be provided. Firstly, the dimensions of all the boundaries in Figure 2 must be given. In most cases the desired value is simply specified directly; however, the dimensions of the cathode spot are determined by assuming a circular spot and a constant current density j_k[13]—together with a given current, these enable the calculation of a representative value for x_{CD}. The location of the centreline of the cathode spot and arc root must also be specified, to locate the boundary regions *BE* and *CD* along the upper surface—unless otherwise stated, these are assumed to be located along the centreline of the model region.

Secondly, values for the constant physical properties of the plasma gas (μ, ρ, κ, C_p), must be provided. These are specified directly by using representative average values for the plasma gas in use over a range of relevant temperatures.

Temperature-dependent values of σ and Q_r are also required. These are specified in the model using a discrete set of values at constant 500 K intervals, between 1 000 K and 33 000 K. The values are obtained from literature[7,14] dealing with physical properties and thermal radiation behaviour of plasmas, and are specific to the composition of the plasma gas and the thermal radiation model (optically thin or thick) considered.

Next, the electrical parameters of the arc must be specified, including the value of j_k on the cathode spot boundary *CD* and the total current provided to the furnace. These in turn define the width of the cathode spot as mentioned above.

Finally, some parameters must be set in order to define the numerical behaviour. The number of finite difference grid points in the *x* and *y* directions, *I* and *J*, must be given. Using these and the dimensions of the region, the spacing between points (δx and δy) can be calculated. The time period to calculate for then completes the data needed by the DC plasma arc model.

Initial conditions

The initial conditions supplied to the model are constant-temperature impulsive start conditions. The velocity (or equivalent field) is set to zero at the start of the calculation, allowing the full evolution of the arc jet to be observed. The initial temperature field is set to a moderately high constant value, 10 000 K, to provide a conductive path for the electric current during the early stages of arc establishment.

Boundary conditions

The spatial boundary conditions necessary to complete the model description are shown in Table I.

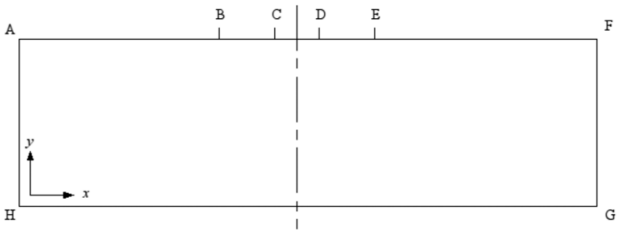

Figure 2—Model geometry and boundaries for 2D cases

Table I

Boundary conditions for plasma arc model

Variable	CD	BC &DE	AH & FG	AB & EF	Gh
v	$v_x = v_y = 0$	$v_x = v_y = 0$	$v_x = v_y = 0$	$v_x = v_y = 0$	$v_x = v_y = 0$
T	$T = T_E$	$T = T_E$	$T = T_W$	$T = T_W$	$T = T_A$
ϕ	$\frac{\partial \phi}{\partial y} = -\frac{j_k}{\sigma}$	$\frac{\partial \phi}{\partial y} = 0$	$\frac{\partial \phi}{\partial x} = 0$	$\frac{\partial \phi}{\partial y} = 0$	$\phi = 0$
A	$A_x = \frac{\partial A_y}{\partial y} = 0$	$A_x = \frac{\partial A_y}{\partial y} = 0$	$A_y = \frac{\partial A_x}{\partial x} = 0$	$A_x = \frac{\partial A_y}{\partial y} = 0$	$A_x = \frac{\partial A_y}{\partial y} = 0$

Model results (2D)

The two-dimensional modelling exercise uses a 'base case' set of parameters, chosen to represent reasonable conditions for a DC plasma arc at pilot plant furnace scale. These are shown in Table II.

The plasma gas is air, and the thermal radiation model used is optically thin. Unless otherwise stated, all the results presented in this section use these values. The base case model was run on an Intel Core2 Q6600 computer with four CPUs and 2GB RAM. The model required 35 961 time step calculations at an average time step size of 0.28 μs, and took approximately two hours to complete.

Arc evolution and behaviour

In the evolution of the model arc, a strong, symmetric, stable jet is initially formed. However, this behaviour is not robust and oscillations in the vicinity of the cathode spot begin to cause the breakdown of the stable arc column into strong, alternating vortices from approximately 0.6 ms into the simulation. The oscillating vortex production near the cathode spot causes the arc column to take on very twisted and sinusoidal shapes. This process is shown in the time sequence in Figures 3 to 6. The plotted temperatures range linearly between 2 000 K (white) and 15 000 K (black), with each discrete colour contour representing a change of 520 K.

As the fields evolve over time, the motion of the arc becomes very turbulent and chaotic. The arc column becomes twisted into a number of unusual shapes and structures. Some examples from further into the simulation are shown in Figures 7 and 8.

It is interesting to observe that small 'parasitic' arcs form on the anode around the main arc jet which emanates from the cathode spot on the electrode above. These are emergent phenomena, as the boundary conditions on the anode surface are entirely isotropic. The parasitic arcs are highly mobile and generally short lived, although they can occasionally interact with one another and combine to form stronger anode arc jets.

In Figure 9, the evolution of the temperature at a location 5 mm below the centre of the cathode spot is plotted. It can be seen that an initial period of smooth, stable behaviour is replaced by very rapidly changing dynamics. The temperature at this location exhibits very large changes in value between 6 000 K and 20 000 K. Figure 10 shows the corresponding variation in arc voltage, measured as the instantaneous maximum value of the electric potential field.

As an indicator of the intensity of the various physical processes in the DC plasma arc model, the maximum instantaneous values of velocity magnitude, temperature, and electric potential may be calculated from the data produced. A time average of these numbers is obtained from the last half of the simulation (5–10 ms), during which the arc motion is

Table II

Base case parameters for 2D plasma arc model

Parameter	Value	Parameter	Value
Region length	0.2 m	j_k	3.5 x 10^7 A/m^2
Region height	0.05 m	Current	500 A
Electrode width	0.05 m	T_W	2000 K
μ	1.307 x 10^{-4} Pa.s	T_A	3000 K
ρ	0.02593 kg/m^3	T_E	4100 K
κ	3.067 W/m.K	Grid dimensions, I x J	1024 x 256
C_p	9420 J/kg.K	Model time	10 ms

Figure 3—Temperature profile, 0.17 ms

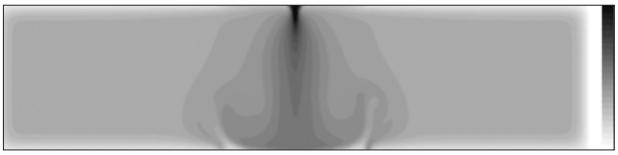

Figure 4—Temperature profile, 0.60 ms

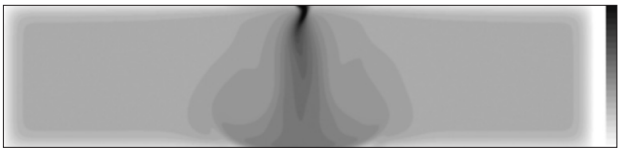

Figure 5—Temperature profile, 0.70 ms

Figure 6—Temperature profile, 0.80 ms

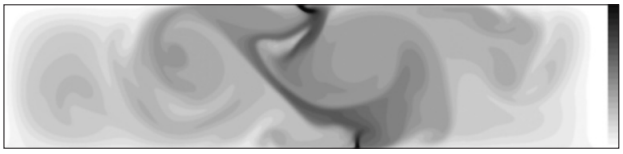

Figure 7—Temperature profile, 7.80 ms

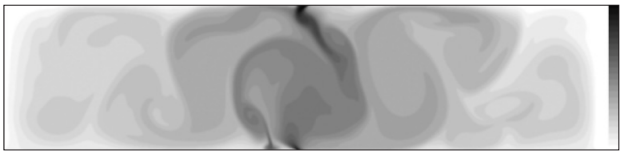

Figure 8—Temperature profile, 9.98 ms

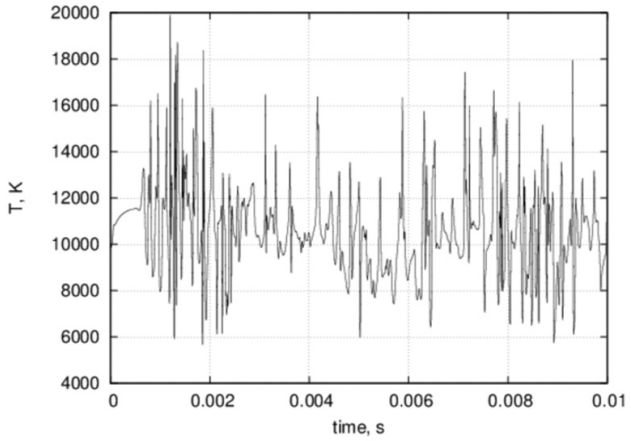

Figure 9—Local temperature variation over time

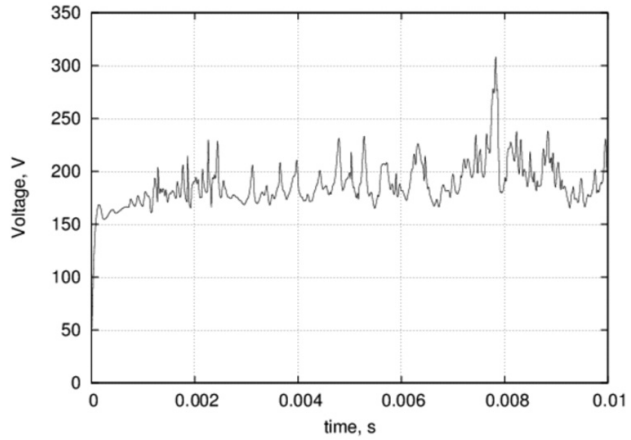

Figure 10—Arc voltage variation over time

generally well established and indicative of long-term behaviour. Instantaneous maximum values are also given for the model at the end of the simulation time (10 ms). These are presented in Table III.

Variation of behaviour with arc length

In order to examine the effect of changing parameters of the DC plasma arc model, the region height (distance from the anode surface to the electrode tip) is altered between 0.0125 m and 0.1 m. This has a significant impact on the Reynolds number of the arc jet flow as well as the total voltage produced by the arc in the model, both of which are seen to increase significantly with region height.

At lower region heights, the arc column becomes more compact and localized, and the degree of turbulence in the region decreases. This results in a striking change in the transient behaviour of the fields in the model, exhibiting regular oscillations at lower region heights and moving to increasingly irregular, chaotic behaviour as the height is increased. This is shown in Figures 11 and 12.

The transition suggests that there is a change in modes between so-called 'brush arc' operation, in which the electrode is positioned very close to the anode surface, and the more usual 'open arc' operation, in which the electrode is positioned well away from the anode. Brush arc operation in DC arc furnaces is traditionally associated with greater stability and is often used during recovery phases—these modelling results may provide some explanation as to why this is the case.

Qualitative comparison with high speed photography

Test work performed in June 2009 on a small-scale pilot plant furnace facility (300 kVA) included running an arc in open air between an exposed graphite electrode and a graphite block serving as the anode. The arc was filmed at 5 000 frames per second using an Olympus high speed digital video camera. The shutter speed was set to 4 μs in order to freeze the arc motion in individual frames of the video. For all results presented here the arc current was 1 kA.

Table III

Maximum values of field variables for base case model

Variable	Maximum value, 5–10 ms average	Maximum value at 10 ms
$\|v\|$	779.4 m/s	744.8 m/s
T	15752 K	15491 K
ϕ	236.9 V	236.7 V

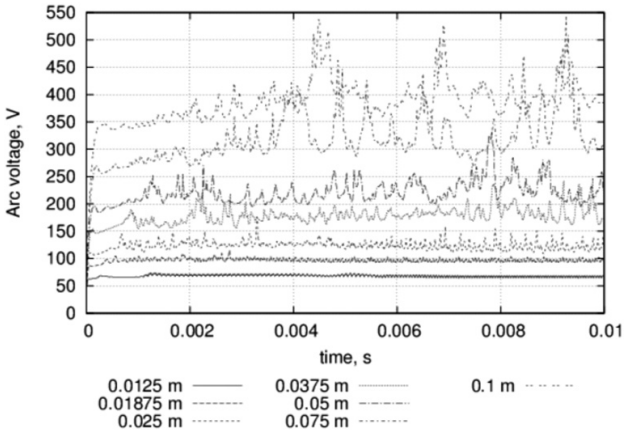

Figure 11—Arc voltage behaviour, various region heights

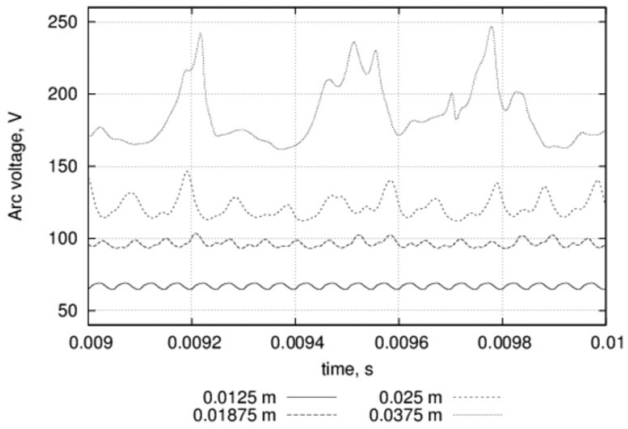

Figure 12—Arc voltage behaviour, various region heights, time between 9 and 10 ms

Of particular interest is the qualitative change in arc behaviour as the electrode position is changed. With the electrode positioned 5 cm above the anode surface, the arc is seen to undergo regular oscillations. This is shown in successive frames from the high speed video in Figures 13 to 16. The images have been converted to black and white and inverted in order to enhance the visibility of the arc column.

As the electrode position is increased to 10 cm, the behaviour changes from steady, regular oscillations to highly irregular unstable behaviour—this is qualitatively similar to the change in behaviour seen in the model. Some examples of this are shown in images from the high speed video in Figures 17 to 20.

It is also interesting to compare the distorted shapes of the arc column in these photographs to the temperature profiles produced by the model (Figures 7 and 8)—many similarities are evident.

The phenomenon of parasitic anode arcs is also clearly visible in the high speed video results. As in the model, the duration of these arcs is very short, milliseconds or less, and they are seen to be highly mobile on the anode surface. Some examples are shown in Figures 21 and 22.

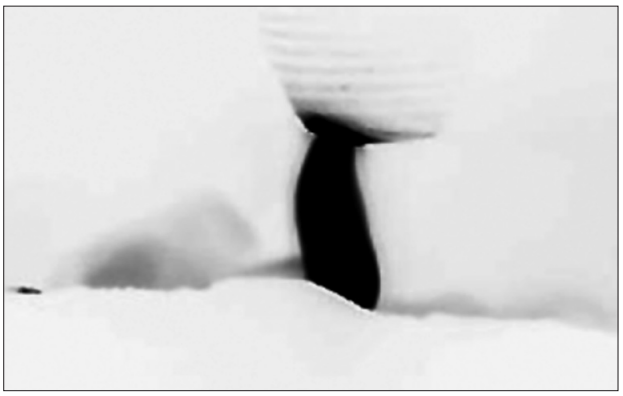

Figure 13—5 cm arc oscillation, frame 49

Figure 14—5 cm arc oscillation, frame 50

Figure 15—5 cm arc oscillation, frame 51

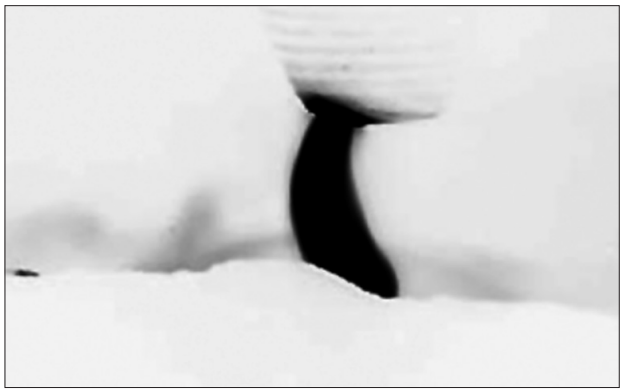

Figure 16—5 cm arc oscillation, frame 52

Figure 17—10 cm arc behaviour, frame 211

Figure 18—10 cm arc behaviour, frame 261

Figure 19—10 cm arc behaviour, frame 362

Figure 20—10 cm arc behaviour, frame 502

Figure 21—10 cm arc, anode arc on right, frame 293

Figure 22—10 cm arc, anode arc on right, frame 367

Model results (3D)

The dynamic plasma arc model is easily extended to three dimensions, where it is particularly useful for more accurate studies of single and multiple arc interaction and behaviour. The electrode surfaces and cathode spots are modelled as circular and may be positioned anywhere on the upper boundary of the model region. Due to the significant increase in computational load, high performance computing resources are generally needed to perform all but the most simple 3D models.

A base case set of parameters is again chosen to represent reasonable conditions for a twin-cathode DC plasma arc furnace at laboratory or small pilot plant scale. These are shown in Table IV. The plasma gas used is air, and the radiation model is optically thin. Viscosity, density, thermal conductivity and heat capacity values are the same as those in Table II, as are parameters j_k, T_W, T_A and T_E.

Arc evolution and behaviour

Much as was observed in the two-dimensional model results, the system initially forms pseudo-steady-state arcs as the initial conditions decay, but as the simulation proceeds they break down and transient motion begins to occur. This process can be seen in Figures 23 to 26, where a side-on view of the 3D region is shown. The plotted temperatures range linearly between 2 000 K (white) and 15 000 K (black), with each discrete colour contour representing a change of 520 K.

The two arcs carrying current in the same direction attract each other magnetically, resulting in the columns bending toward each other (and the centre of the furnace)—this can clearly be seen in Figures 23 to 26.

Due to the substantially lower current used for each of the two arcs in the 3D case, the subsequent transient behaviour is not as chaotic as seen in the 2D base case and manifests as more regular oscillations. This can be seen in the temperature trends at locations 5 mm below the centre of the two arcs' cathode spots, shown in Figures 27 and 28. 'x = 0.08 m' refers to the arc on the left, 'x = 0.12 m' refers to the arc on the right.

Table IV

Base case parameters for 3D plasma arc model

Parameter	Value	Parameter	Value
Region length	0.2 m	Current (arc 1)	250 A
Region width	0.1 m	Current (arc 2)	250 A
Region height	0.05 m	Arc separation	0.04 m
Electrode diameter	0.05 m	Grid resolution, I x J x K	384 x 192 x 96
Number of arcs	2	Model time	10 ms

Figure 23—Temperature profile, 0.5 ms

Figure 24—Temperature profile, 1.0 ms

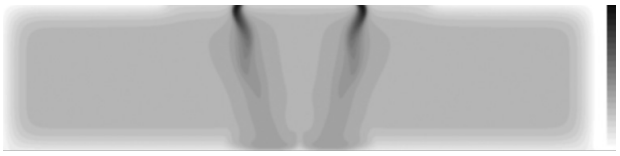

Figure 25—Temperature profile, 1.5 ms

Figure 26—Temperature profile, 2.0 ms

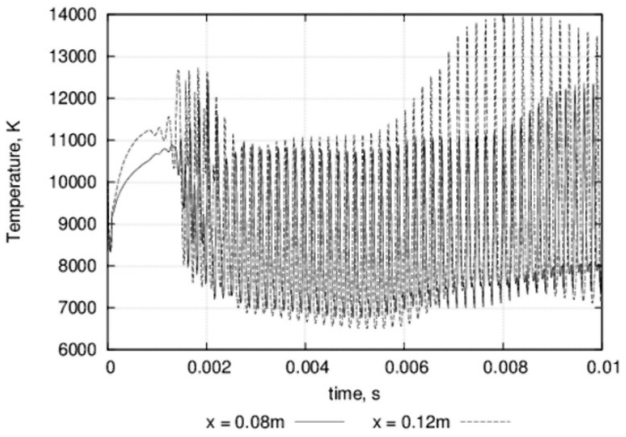

Figure 27—Local temperature variation over time

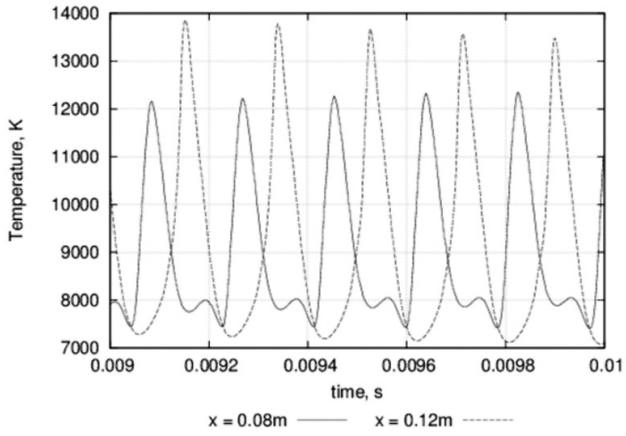

Figure 28—Local temperature variation, last 1 ms

In three dimensions, the transient behaviour is associated with a precession of the arc jet around the location of the cathode spot. At lower currents, this precession occurs at approximately constant rate and results in the formation of a helical shape in the arc column. This is visible in Figures 29 and 30, where a top-down view of the 3D region is shown.

Variation of behaviour with arc separation

As in 2D, certain parameters used for the model can be varied independently in order to gain an understanding of their effect on the plasma arc system. A variable of considerable interest to twin-electrode furnace designers is the spacing between the electrodes (and hence arcs). In order to study this, the separation in the model was varied between 10 and 2 cm. The results are shown in Figures 31 to 35, where a side-on view of the temperature field at the end of each simulation is shown.

As the electrode separation distance decreases, the magnetic attraction between the two arc columns increases, and they begin to bend more toward each other. At 6 cm, the arcs are still (barely) two distinct entities, but by 4 cm, the flow and temperature fields begin to merge along at least part of their length, and by 2 cm, the arcs have joined quite near to the cathode spots to form a single, larger arc column. The helical patterns formed by the transient motion of the jet near the cathode spots is most clearly visible in the arc structures at large separation distances. As the arcs move closer together, the interaction between them begins to affect the structure, producing more irregular shapes.

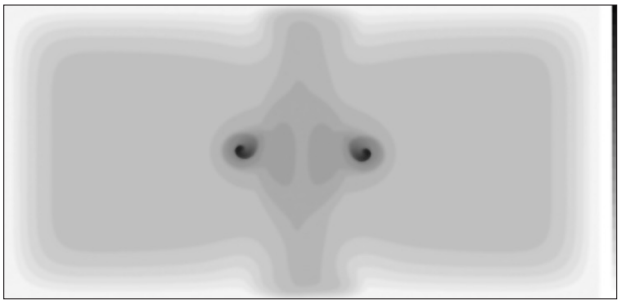

Figure 29—Temperature profile, 5.0 ms

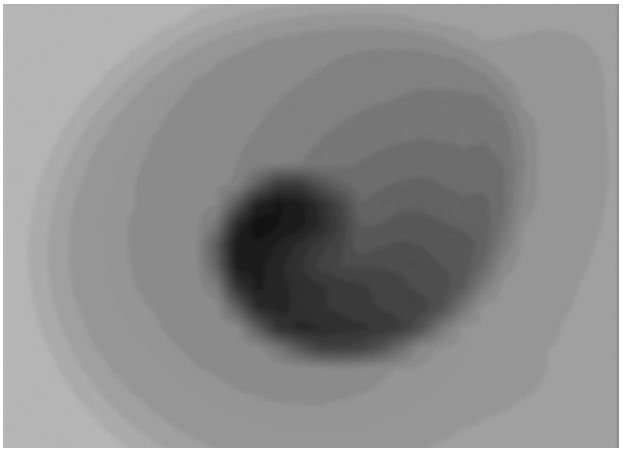

Figure 30—Close-up showing helical arc structure

Figure 31—Temperature profile, separation 10 cm

Figure 32—Temperature profile, separation 8 cm

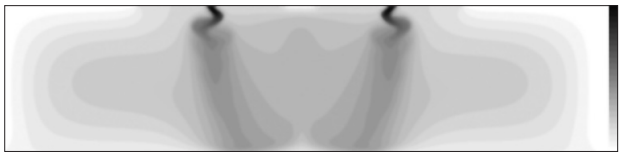

Figure 33—Temperature profile, separation 6 cm

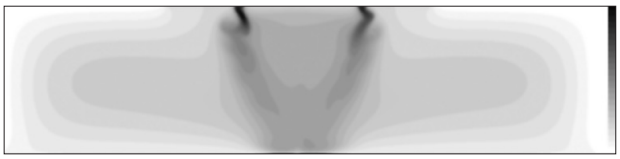

Figure 34—Temperature profile, separation 4 cm

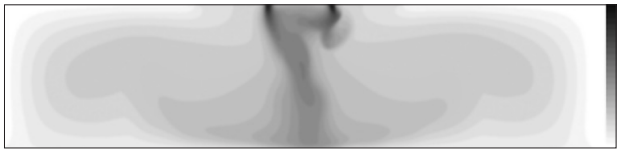

Figure 35—Temperature profile, separation 2 cm

The degree of deflection of the arc columns toward each other can be quantified by measuring the distance between the local peak values of temperature near to the anode surface. Performing this calculation for each simulation at time 10 ms gives the relationship in Figure 36, showing the amount that the arc jets have moved toward each other from their original starting points at the cathode spots.

The behaviour at 2 cm is not included on this graph, since at this point the arcs have already merged together (arc column separation = 0). It is clear that bringing two arcs closer together causes them to bend toward each other increasingly strongly.

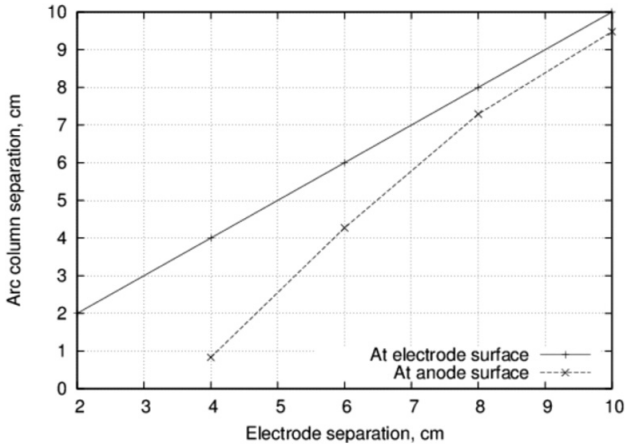

Figure 36—Distance between centrelines of arc jets near to anode vs. original separation

Conclusions and recommendations

A mathematical formulation of the fundamental physical processes occurring in DC plasma arcs has been developed and approximated with appropriate numerical methods. The aims of designing a model suitable for operation at high spatial and temporal resolutions were used to guide the choice of the numerical methods used. Several novel concepts are associated with the development and implementation of the model in this work, notably the use of cartesian grids two dimensions and the strong focus on unsteady-state equations and methods to capture the dynamics and qualitative behaviour of DC plasma arc systems on very short timescales.

Selected results from the two- and three-dimensional models of plasma arcs have been presented. These have demonstrated a number of interesting qualitative features, including transitions between steady and unsteady behaviour as the arc is established, spontaneous formation of transient anode arcs, and change in temporal behaviour between regular oscillations and turbulent chaotic behaviour as a result of altering process parameters such as electrode position and arc current. Comparisons with experimental results from high speed photography of real arcs show a number of similar effects. Multiple-arc systems were also briefly examined, demonstrating arc deflection and interaction as well as helical structure formation in the arc column.

A number of enhancements and extensions could be applied to the DC plasma arc model in order to greatly increase its value as a research tool. Further work on refinement and optimization of the algorithmic aspects of the model is of some importance, since strongly-coupled multi-physics problems such as this are very demanding on computing resources. In addition, generalizations of the models can be contemplated—inclusion of temperature-dependent physical properties of the plasma fluid would improve the model's accuracy, and for the study of larger arcs at higher currents, both compressible fluid flow models and induced current effects in the electromagnetism model would need to be considered.

Acknowledgements

The authors would like to thank Mintek, the CSIR Centre for High Performance Computing, the University of Cape Town, and VIP Technologies/Olympus Industrial for their involvement and assistance with this work.

References

1. Barcza, N.A., Curr, T.R., Winship, W.A., and Heanley, C.P. The production of ferrochromium in a transferred-arc plasma furnace, *39th Electric Furnace Conference proceedings*, 1982, pp. 243–260.
2. Schoukens, A.F.S., Denton, G.M., and Jones, R.T. Pilot plant production of prime western grade zinc from lead blast furnace slags using the Enviroplas process, *Proceedings of the Third International Symposium on Recycling of Metal and Engineered Materials*, 1995, pp. 857–868.
3. Kotze, I.J. Pilot plant production of ferronickel from nickel oxide ores and dusts in a DC arc furnace, *Minerals Engineering*, vol. 15, no. 12, Supplement 1, November 2002, pp. 1017–1022.
4. Jones, R.T. and Kotze I.J., DC arc smelting of difficult PGM-containing feed materials, *Proceedings of the SAIMM International Platinum Conference*, 2004, pp 33–36.
5. Schoukens, A.F.S., Abdel-latif, M., and Freeman, M.J., Technological breakthrough of the Mintek Thermal Magnesium Process, *Journal of the South African Institute of Mining and Metallurgy*, vol. 106, no. 1, 2006, pp. 25–29.
6. Maecker, H. Plasmaströmungen in Lichtbögen infolge Eigenmagnetische Kompression, *Zeitschrift für Physik*, vol. 141, 1955, pp. 198–216.
7. Boulos, M.I., Fauchais, P., and Pfender, E. *Thermal plasmas: fundamentals and applications*, vol. 1, Plenum Press, 1994.
8. Haus, H.A. and Melcher, J.R., *Electromagnetic fields and energy*, Prentice-Hall, 1989.
9. E, W. and Liu, J.G. Gauge method for incompressible flows, *Communications in Mathematical Sciences*, vol. 1, no. 2, 2003, pp. 317–332.
10. E, W. and Liu, J.G. Vorticity boundary condition and related issues for finite difference schemes, *Journal of Computational Physics*, vol. 124, 1996, pp. 368–382.
11. http://www.fftw.org
12. Brandt, A. Multi-level adaptive solutions to boundary-value problems, *Mathematics of Computation*, vol. 31, no. 138, 1977, pp. 333–390.
13. Bowman, B. Properties of arcs in DC furnaces, *52nd Electric Furnace Conference proceedings*, 1995, pp. 111–120.
14. Naghizadeh-Kashani, Y., Cressault, Y., and Gleizes, A. Net emission coefficient of air thermal plasmas, *Journal of Physics D: Applied Physics*, vol. 35, 2002, pp. 2925–2934. ◆